

Polarization-Independent Wide-Angle Terahertz Metamaterial Absorber: Design, Fabrication and Characterization

Khwanchai Tantiwanichapan*, Anucha Ruangphanit, Wittawat Yamwong, Rattanawan Meananeatra, Arckom Srihapat, Jia Yi Chia, Napat Cota, Kiattiwut Prasertsuk, Patharakorn Rattanawan, Chayut Thanapirom, Rungroj Jintamethasawat, Kittipong Kasamsook, and Nipapan Klunngien

Abstract—A metamaterial absorber in the Terahertz (THz) range is simulated and experimentally investigated in this work. The desired absorption frequency, efficiency, and bandwidth can be tuned by changing the metal and dielectric geometric parameters. An absorption greater than 85% for TM polarized light with an incident angle up to 70° at any azimuthal direction is observed in a circular disc THz metamaterial structure. By adjusting the dielectric silicon dioxide (SiO_2) thickness to $4\ \mu\text{m}$, an optimal absorption greater than 95% can be achieved at a resonance frequency of 0.97 THz. The experimental results also indicate that using Titanium (Ti) as a metamaterial metal layer provides four times broader absorption bandwidth than Aluminium (Al). This study, which works on polarization-insensitive and wide-angle metamaterial absorbers, can be fundamentally applied to many THz applications including THz spectroscopy, imaging, and detection.

1. INTRODUCTION

A metamaterial is a geometrically and structurally designed composite material, which exhibits extraordinary properties not found in intrinsic materials such as negative refractive index, backward wave propagation, and diffraction-limit breaking imaging [1–3]. These exceptional properties enable many exciting advancements in various applications including subwavelength waveguiding, invisible cloaking, superlenses, and sensors [4–7]. One of the most widely studied metamaterial applications is metamaterial absorber (MA). MA is an electromagnetic energy consuming device that couples electric and magnetic fields to localized absorption regions. This concept is very important for the applications in developing sensing materials, spectroscopy, thermal-based detection, and imaging [8–11].

Ever since MA was first experimentally demonstrated by Landy et al. [12] in 2008, several theoretical and experimental works have been done at various electromagnetic wavelengths in microwave to optical range [13–16]. Many researchers have focused on different aspects of the MA with different approaches, especially in THz spectral range where it is difficult to find materials in nature. Some groups have worked on the multi-band THz MAs [17–24]. For example, Tao et al. [17] experimentally showed a bi-layer THz MA composed of electrical ring resonator on cut wire in a reflection mode for the first time. Others have developed broadband THz MAs using methods such as a stack of many metamaterial layers, different material sizes in a unit cell, and a special pattern design in a unit cell [25–28]. In order to achieve frequency-adjustable absorption in a single device, the THz MAs with resonance frequency tunability are widely studied with different techniques such as those in the photoexcitation, liquid crystal, and thermal-based MAs [29–33].

Received 16 August 2019, Accepted 17 November 2019, Scheduled 30 November 2019

* Corresponding author: Khwanchai Tantiwanichapan (khwanchai.tantiwanichapan@nectec.or.th).

The authors are with the National Electronics and Computer Technology Center, 112 Thailand Science Park, Phahonyothin Road, Khlong Nueng, Khlong Luang, Pathum Thani 12120, Thailand.

Other important properties for the practical THz applications are polarization-independence and wide-angle operability, which have been studied recently [34, 35]. These properties are crucial to enable the development of devices to be functional with minimal configurations. Additionally, since the availability of the THz sources and devices are commercially limited, these properties enable easier compatibility with the most currently available sources. In this work, we have simulated and experimentally investigated the effects of the related parameters on a simple circular-disc antenna THz MA. Our results indicate that by engineering the geometrical parameters, we can achieve a tunable polarization-insensitive response frequency at any incident angle. In order to get a nearly perfect absorption, the MA impedance is optimized by varying the dielectric layer thickness in both simulations and experiments. Moreover, we show that the absorption bandwidth can be simply designed by appropriate selection of the metal type used for the circular discs. Compared with other absorber technologies, the geometrical and structural design of our MA offers many advantages. First, our MA can be designed as a nearly perfect absorber with a thickness less than $\lambda/50$, which is remarkably smaller than that of current conventional homogeneous absorbers [36, 37]. Second, our operational angle is broader than that of cylindrical or lossy particles absorbers [38, 39]. Moreover, the MA in this work is polarization-insensitive, which is not found in some of the existing material-based absorbers [40]. In addition, all materials and fabrication processes applied in this work are based on industrial CMOS technology, which is cost-effective and has great potential in mass production compared with other technologies.

2. STRUCTURE, DESIGN AND METHOD

The THz absorption devices designed in this work are based on Metal-Insulator-Metal (MIM) metamaterial structures. They consist of an Al metal layer over a SiO_2 on AlCuSi metal ground plane, as depicted in Figs. 1(a) and 1(b). The top metal layer is designed as a 2D array of periodic circular discs for symmetry purposes, in order to enable polarization-insensitivity. There are two periods of the metallic disc pattern that are explored; $100\ \mu\text{m}$ for disc of diameter $d = 40\text{--}90\ \mu\text{m}$ and $200\ \mu\text{m}$ for disc of diameter $d = 100\text{--}180\ \mu\text{m}$. Many parameters, including the size and type of metal and dielectric layers, were first numerically simulated by using the commercial finite-difference time-domain (FDTD) software. These initial simulation results were analyzed to investigate the effect of each parameter on

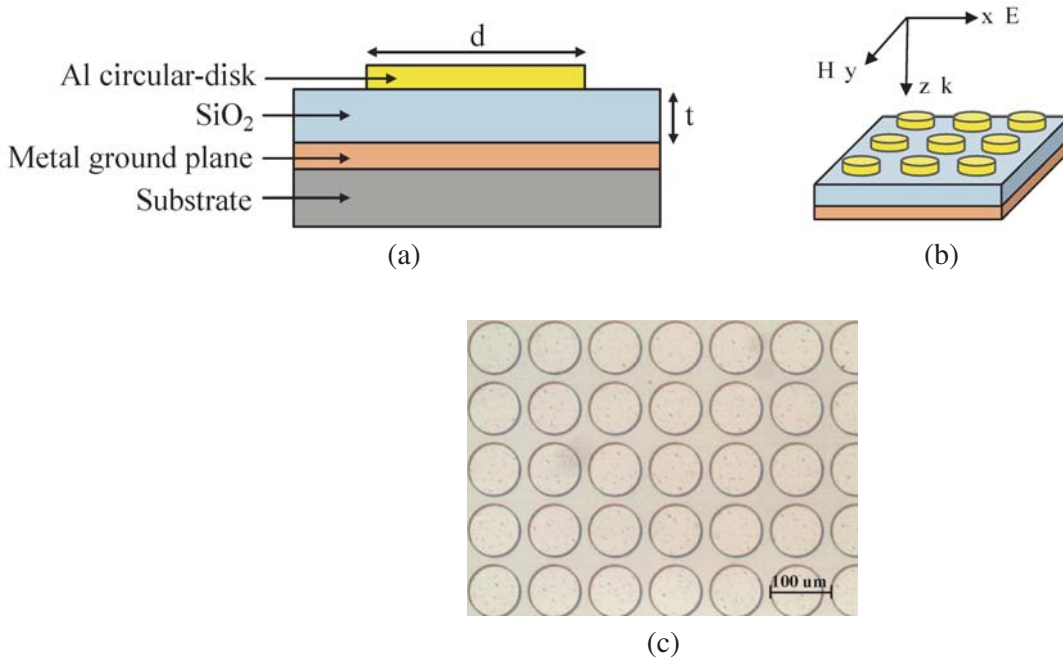


Figure 1. (a)–(b) THz MA design structure and (c) an optical image of the fabricated MA.

the THz metamaterial absorption and were used as a guideline for device fabrication. In addition, these simulations and their corresponding experimental results are compared in order to understand the behaviors of this THz MA structure.

The fabrication process, implemented in this work, complied with a standard CMOS microfabrication technology. First, a stack of Ti/TiN/AlCuSi with the thicknesses of 30, 80 and 500 nm was sputtered, respectively as a ground plane on a commercial Si wafer. On top of those layers, a SiO₂ dielectric layer was deposited by plasma-enhanced chemical vapor deposition (PECVD). Finally, we patterned Al circular-disc arrays by using sputtering, standard photolithography and reactive ion etching (RIE) process, as shown in Figs. 1(a) and 1(b). Fig. 1(c) shows an optical image of the fabricated Al circular-disc MA with a diameter of $d = 90 \mu\text{m}$ on SiO₂ dielectric layer.

To analyze the absorption of the THz MA device, THz Time-Domain Spectroscopy (THz-TDS) was performed in the reflection mode, as shown in Figs. 2(a) and 2(b). The THz-TDS emitter Photoconductive Antenna (PCA) was mounted on two parabolic mirrors in such a way as to ensure that the emitted beam was focused on the MA device. A linear polarizer was placed at the emitter side after the second mirror for TE and TM polarization adjustments. By rotating a linear polarizer in a horizontal direction (parallel to the optical table), we could obtain TM polarized incident beam. On the other hand, incident TE polarized light could be achieved by rotating a linear polarizer 90 degree, which was a vertical direction (normal to the optical table). The receiver PCA was mounted on two similar parabolic mirrors as same as in the emitter side. Both emitter and receiver sets were mounted on a rotatable stage for adjusting the incident angle θ . Due to limitations of our experimental setup, the

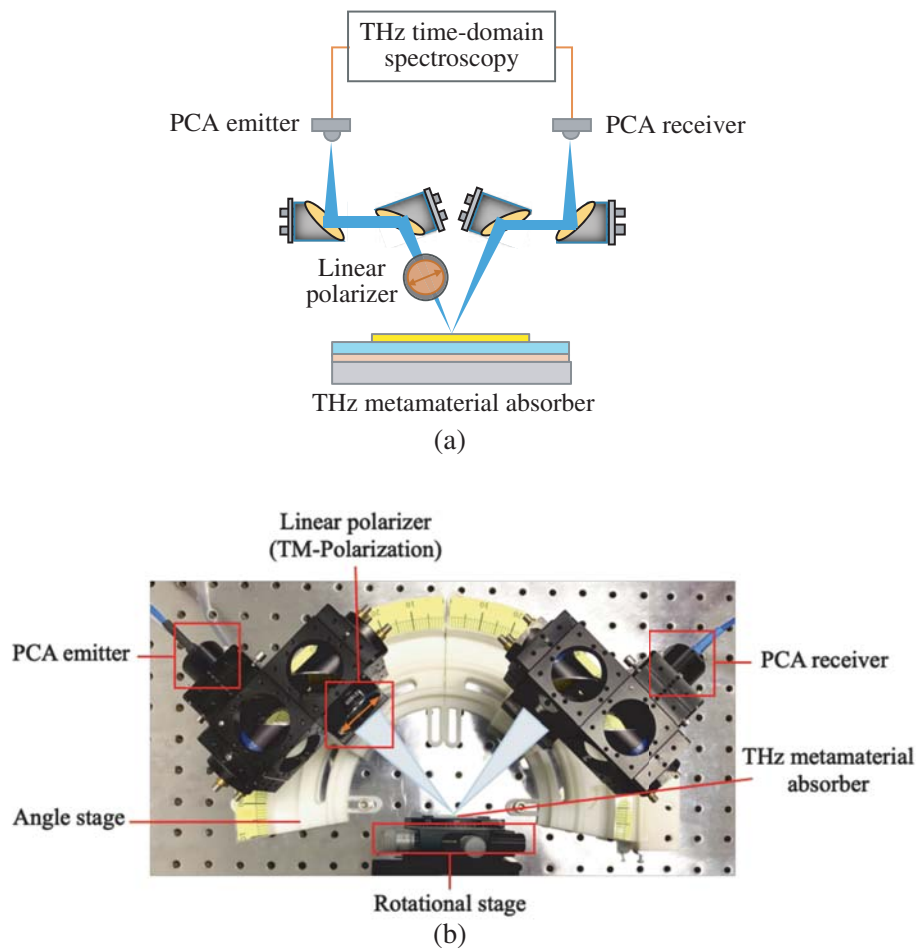


Figure 2. (a) Absorption measurement setup diagram using the THz-TDS and (b) top view of the actual experimental setup.

minimum angle of incidence we could achieve was 30° . The MA device was placed on another rotational stage allowing for adjustment of the azimuthal angle of incidence ϕ . Note that the absorption signal from the THz MA was normalized to absorption of 200 nm Au ground plane reflector.

3. RESULTS AND DISCUSSION

In this work, the effect of metal diameter size on signal absorption in the THz MA has been investigated. Fig. 3(a) presents an absorption spectrum of circular-disc MAs for different sizes of the metal diameters d on a SiO_2 dielectric layer with a thickness of $t = 4 \mu\text{m}$. Our experimental results are in good agreement with numerical simulations, as shown in Fig. 3(a). The slight disparities in both the absorption frequency and absorption efficiency can be attributed to the imperfect metamaterial fabrication and the measurement limitations. The diameter of the circular discs in the experimental is slightly smaller than the simulation design due to inherent limitations in the fabrication process. Moreover, due to the lower THz signal-to-noise ratio at higher frequency in the THz-TDS, the absorption at higher frequency has large discrepancies in the measurement. As we can see from the plot, the narrow-bandwidth single-frequency absorption can be tuned in the range of 0.42–2.20 THz by varying the metal disc diameter from 180 to 40 μm . The variation of absorption efficiency at each metal diameter is due to an optical impedance mismatch of each MA resulting in a different reflection at the interface between MA and free space. The absorption strength of the diameter range $d = 40\text{--}90 \mu\text{m}$ is relatively higher than that of the diameter range $d = 100\text{--}180 \mu\text{m}$ because of a difference in periodicity, which is $100 \mu\text{m}$ for the former and $200 \mu\text{m}$ for the latter.

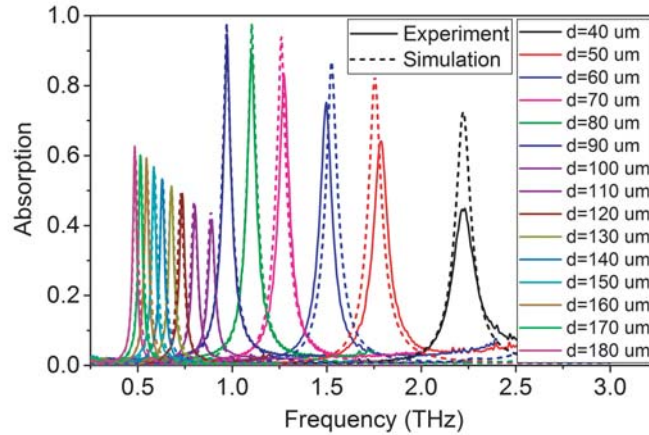


Figure 3. Simulated (dashed line) and measured (solid line) absorption results of the THz MA with the structure shown in Fig. 1(a).

In order to understand the physical mechanism of this THz MA, the electric field distribution (E_z), magnetic field distribution (H_x), and the surface currents from the simulation are analyzed and plotted in Fig. 4. All subfigures show the numerical results at the resonance frequency of the device with a disc diameter of $d = 90 \mu\text{m}$, which is a nearly perfect absorption MA at 0.97 THz. Fig. 4(a) shows the separation of positive and negative electric fields E_z at each side of the interface between metal circular disc and SiO_2 . This simulated result indicates the excitation of electric dipolar resonance from the opposite charges accumulated at the opposite sides in the THz MA [27, 30]. Figs. 4(c) and 4(d) present the surface currents at the metal circular disc on the top and the metal ground plane at the bottom. The anti-parallel surface currents confirm the existence of magnetic resonance induced in the THz MA between these two metal layers. Moreover, the magnetic field distribution (H_x), as depicted in Fig. 4(b), demonstrates the existence of confined magnetic resonance between the top circular disc layer and the bottom ground plane. These electric dipolar resonance and magnetic resonance lead to the absorption of electromagnetic incident signal with the THz MA.

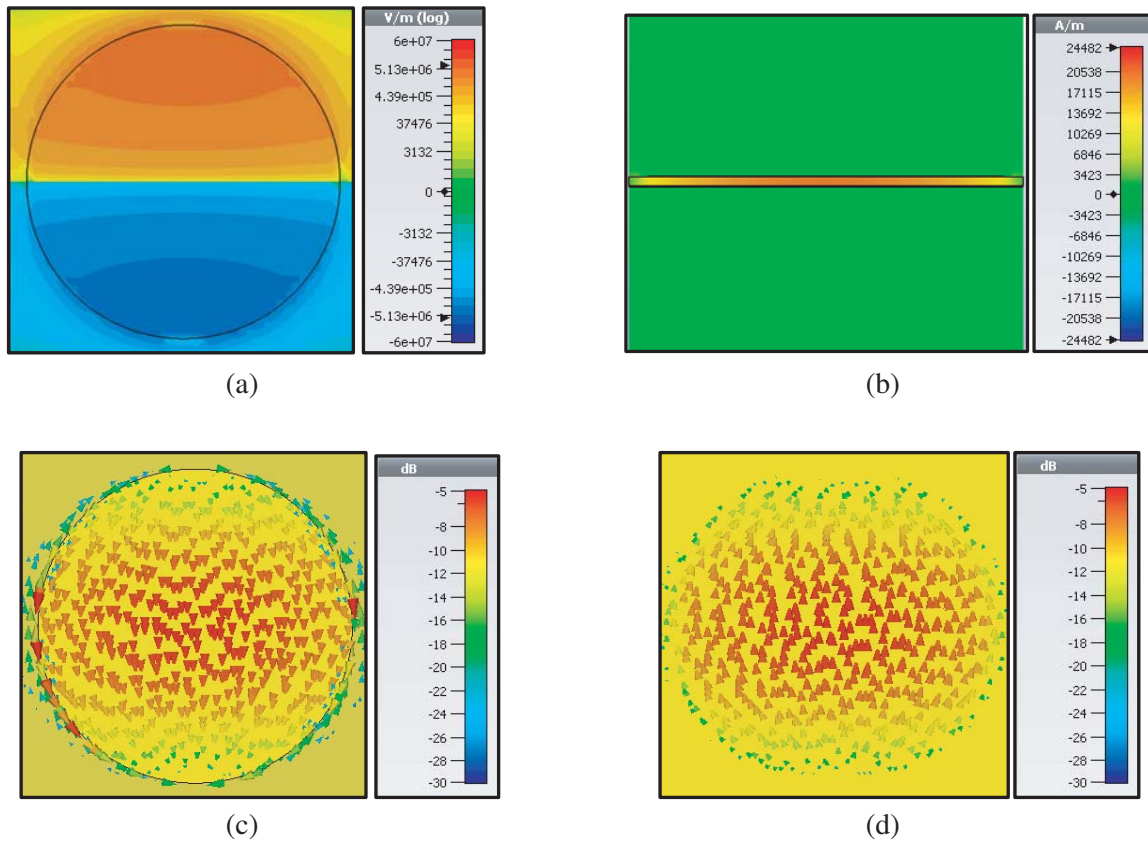


Figure 4. (a) Electric field distribution (E_z), (b) magnetic field distribution (H_x) and (c)–(d) surface currents on the top of circular disc and at the bottom of ground plane from the simulation of $d = 90 \mu\text{m}$ disc.

The impedance mismatch is investigated in more details by changing the thickness of the dielectric layer. We fabricated THz MAs with SiO_2 thicknesses of $t = 2, 3$ and $4 \mu\text{m}$ and different metal disc diameters. The absorption efficiency is plotted in Fig. 5(a), demonstrating that when the SiO_2 thickness t increases, the absorption efficiency gets higher in all sample diameters. The signal greater than 95% can be absorbed by the device with SiO_2 thickness of $t = 4 \mu\text{m}$ and metal diameter of $d = 90 \mu\text{m}$. This result can be interpreted from a normalized impedance extracted from the simulation [15, 26]. For a sample with $d = 90 \mu\text{m}$ and SiO_2 thickness of $t = 4 \mu\text{m}$, the imaginary and real parts of its normalized impedance are 0.04 and 0.95 respectively at a resonance frequency of 0.932 THz, as presented in Figs. 5(b) and 5(c). The experimental and simulated results are in good agreement with the normalized impedance of a perfect absorber whose imaginary and real parts are required to be 0 and 1 respectively, i.e., the impedance of a perfect absorber matches that of free space impedance ($Z = Z_0$). In comparison, other thicknesses $t = 2 \mu\text{m}$ and $3 \mu\text{m}$, which have imaginary and real parts mismatching from the free space impedance, exhibit the lower absorptions. From this analysis, it can be concluded that one can achieve a perfect absorption in any MA design by adjusting the thickness of its dielectric material to match its impedance that of free space.

The absorptions at different incident angles for TM and TE polarizations are explored with a THz MA of diameter $d = 90 \mu\text{m}$ on a $4 \mu\text{m}$ thick SiO_2 layer, which is a nearly perfect absorption device. As presented in Figs. 6(a) and 6(b), the experimental results show an absorption of more than 85% for TM waves at the invariable resonance frequency of 0.97 THz for all angles of incidence θ from 30° to 70° . On the other hand, the absorption for TE waves decreases as the incident angle increases, still with more than 60% of absorption at the incident angle of 60° . These results are analyzed further by simulating the absorption in TM and TE modes at an incident angle of 70° . In Figs. 6(c) and 6(d),

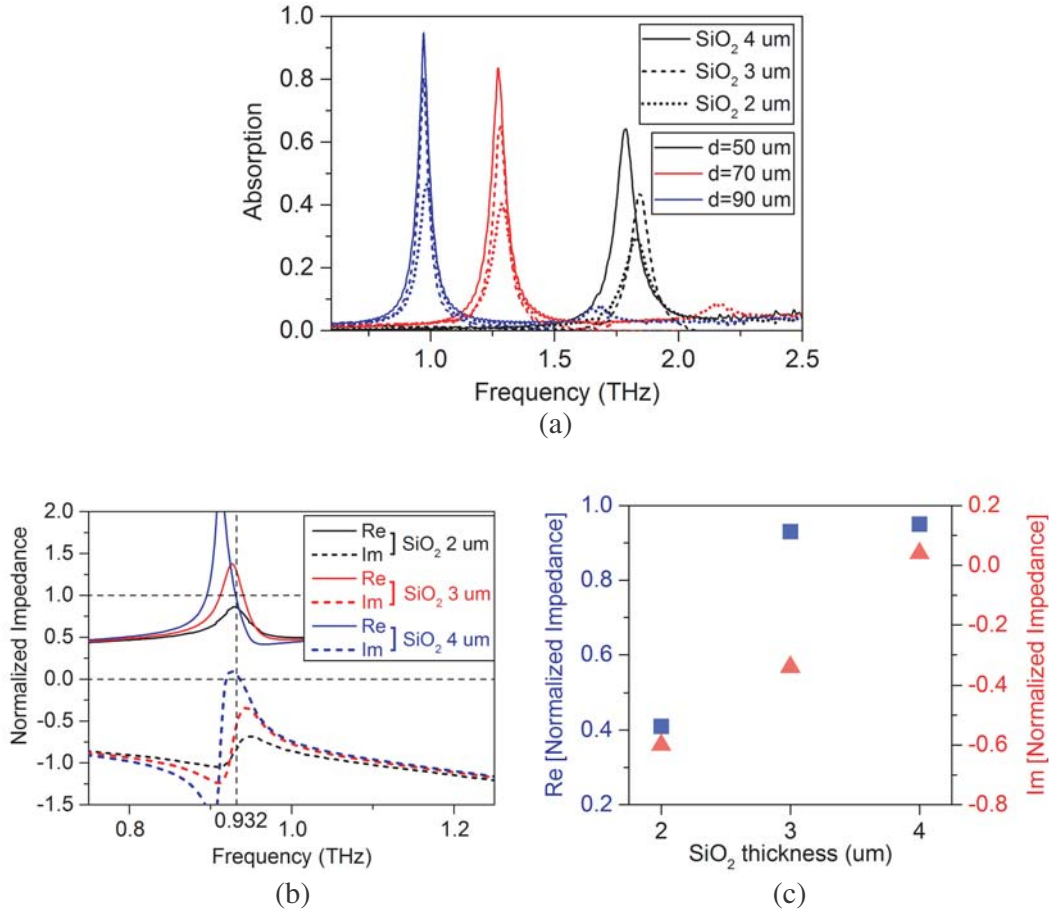


Figure 5. (a) The absorption with different SiO₂ thicknesses t and (b)–(c) real and imaginary parts of normalized impedance of $d = 90 \mu\text{m}$ for different SiO₂ thicknesses of $t = 2, 3,$ and $4 \mu\text{m}$.

with the same scale, the electric field distribution $|E|$ of TM wave is visibly larger than $|E|$ of TE wave. Indeed, the maximum calculated electric field in TM polarization is $4.36 \times 10^6 \text{ V/m}$, which is larger than $3.07 \times 10^6 \text{ V/m}$ in TE polarization. This is due to the higher coupling efficiency of the incident electric field to MA in the TM mode, which is in agreement with the experimental absorption result shown in Figs. 6(a) and 6(b) (i.e., the absorption of TM is 0.85 which is larger than 0.45 of TE wave, at $\theta = 70^\circ$).

Another important parameter for a practical operation, the incident azimuthal angle φ in TM mode, is also investigated at $\theta = 30^\circ$. We observe an absorption higher than 95% at φ from 0° to 90° , as presented in Fig. 6(e). A deviation of absorption frequency of less than 5 GHz at the resonance frequency of 0.97 THz can be achieved in this metamaterial structure. The independency of azimuthal angle φ on the absorption can be attributed to the symmetric design of our circular disc pattern.

In order to further investigate the absorption behavior of the MA, we studied two types of metal, which were Ti and Al of 200 nm thickness fabricated on different samples with diameters of $d = 70$ and $90 \mu\text{m}$ on a SiO₂ dielectric layer with a thickness of $t = 3 \mu\text{m}$. Fig. 7(a) shows the different absorption results from each metal type device. Al provides narrower and higher absorption. In contrast, the broader spectrum and lower absorption can be obtained with Ti. This can be attributed to the fact that Ti is a highly loss material with a high absorption coefficient (i.e., large imaginary part of refractive index) compared to Al. Indeed, the broadening bandwidth is due to the combination of the localized surface plasmon (LSP) broadband absorption in this highly loss material and the propagating surface plasmon (PSP) absorption, as discussed by Ding et al. [15] and Lei et al. [41]. On the other hand, only normal PSP contributes to the observed narrow bandwidth absorption in Al.

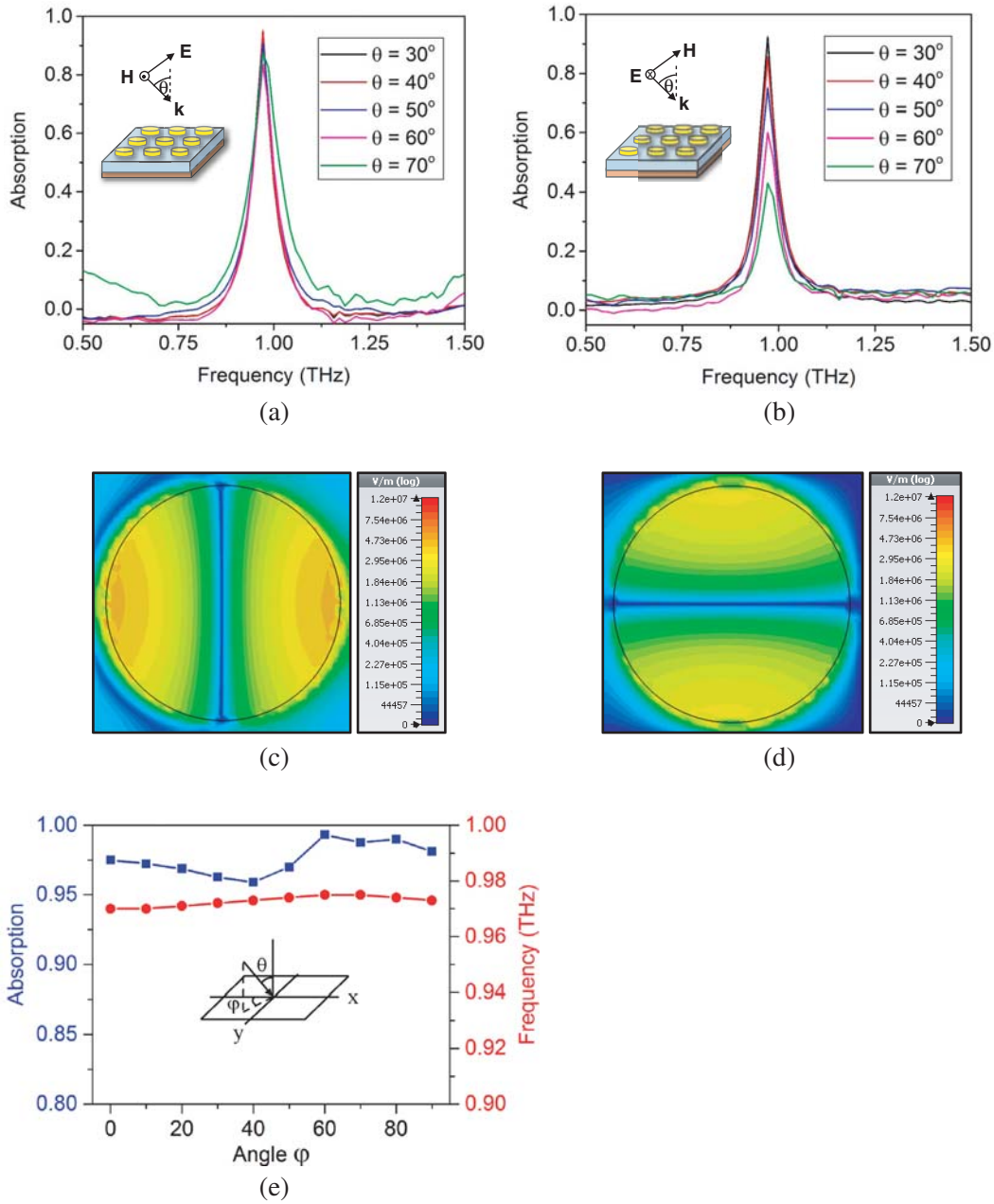


Figure 6. (a) The absorption at different incident angles θ for the TM polarization, and (b) the TE polarization, (c) electric field distribution $|E|$ at the MA interface from the simulation of TM, and (d) TE at $\theta = 70^\circ$, and (e) the absorption and resonance frequency at different azimuthal angles φ .

In order to better understand the absorption bandwidth of each metal, we fabricated Ti on a thicker SiO_2 layer, resulting in a higher absorption efficiency. The absorption from Ti on a $10\ \mu\text{m}$ thick SiO_2 dielectric layer is approximately on the same magnitude as Al on a $3\ \mu\text{m}$ thick SiO_2 layer, as depicted in Fig. 7(b). The Full Width at Half Maximum (FWHM) bandwidth of Ti (around $0.2\ \text{THz}$) is remarkably broader than that of Al ($0.05\ \text{THz}$) with the metal diameter of $d = 90\ \mu\text{m}$. Based on this result, we can conclude that the metal material is another important parameter in designing for a desired absorption bandwidth in THz MAs.

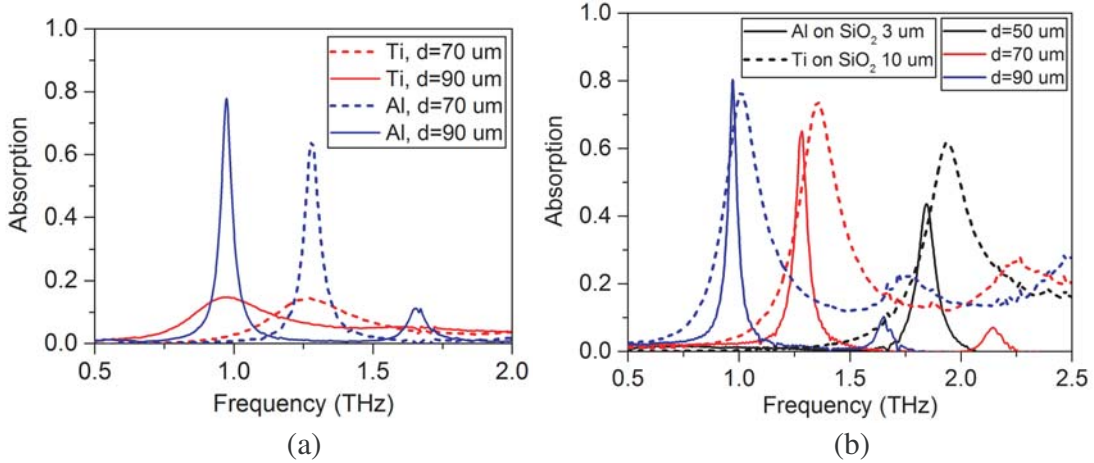


Figure 7. (a) The absorption of MAs with different metals, and (b) the absorption of Al on a SiO₂ layer with $t = 3 \mu\text{m}$ compared with Ti on a SiO₂ layer with $t = 10 \mu\text{m}$.

4. CONCLUSION

The effect of various parameters on THz metamaterial absorption is numerically and experimentally studied in this work. With a simple circular disc pattern MA, an absorption of more than 85% for TM polarization at the incident angles up to 70° can be achieved for any azimuthal angle. A resonance frequency ranging from 0.42 to 2.2 THz is obtained by geometrically tuning the circular disc diameter from $40 \mu\text{m}$ to $180 \mu\text{m}$. Moreover, this study further contributes to MA design for any desired absorption efficiency and bandwidth by showing the effect of customizing the thickness of dielectric and type of metal. This result can be a principle guideline for designing polarization-independent and wide-angle operable MAs in the THz regime.

REFERENCES

- Shelby, R. A., D. R. Smith, and S. Schultz, "Experimental verification of a negative index of refraction," *Science*, Vol. 292, 77–79, 2001.
- Hasar, U. C. and J. J. Barroso, "Retrieval approach for determination of forward and backward wave impedances of bianisotropic metamaterial," *Progress In Electromagnetics Research*, Vol. 112, 109–124, 2011.
- Belov, P. A., Y. Hao, and S. Sudhakaran, "Subwavelength microwave imaging using an array of parallel conducting wires as a lens," *Phys. Rev. B*, Vol. 73, 033108, 2006.
- Duan, Z., Y. Wang, X. Mao, W.-X. Wang, and M. Chen, "Experimental demonstration of double-negative metamaterials partially filled in a circular waveguide," *Progress In Electromagnetics Research*, Vol. 121, 215–224, 2011.
- Lee, Y., S. J. Kim, H. Park, and B. Lee, "Metamaterials and metasurfaces for sensor applications," *Sensors*, Vol. 17, 1726, 2017.
- Schurig, D., J. J. Mock, B. J. Justice, S. A. Cummer, J. B. Pendry, A. F. Starr, and D. R. Smith, "Metamaterial electromagnetic cloak at microwave frequencies," *Science*, Vol. 314, 977–980, 2006.
- Alitalo, P., C. A. Valagiannopoulos, and S. A. Tretyakov, "Simple cloak for antenna blockage reduction," *IEEE Int. Antennas Propag. Symposium*, 2011.
- Zou, H. and Y. Cheng, "Design of a six-band terahertz metamaterial absorber for temperature sensing application," *Opt. Mater.*, Vol. 88, 674–679, 2019.

9. Xu, W., L. Xie, J. Zhu, X. Xu, Z. Ye, C. Wang, Y. Ma, and Y. Ying, "Gold nanoparticle-based terahertz metamaterial sensors: Mechanisms and applications," *ACS Photonics*, Vol. 3, 2308–2314, 2016.
10. Wang, B. X., X. Zhai, G. Z. Wang, W. Q. Huang, and L.-L. Wang, "A novel dual-band terahertz metamaterial absorber for a sensor application," *J. Appl. Phys.*, Vol. 117, 014504, 2015.
11. Escorcia, I., J. Grant, J. Gough, and D. R. Cumming, "Uncooled CMOS terahertz imager using a metamaterial absorber and pn diode," *Opt. Lett.*, Vol. 41, 3261–3264, 2016.
12. Landy, N. I., S. Sajuyigbe, J. J. Mock, D. R. Smith, and J. Padilla, "Perfect metamaterial absorber," *Phys. Rev. Lett.*, Vol. 100, 207402, 2008.
13. Tao, H., E. A. Kadlec, A. C. Strikwerda, K. Fan, W. J. Padilla, R. D. Averitt, E. A. Shaner, and X. Zhang, "Microwave and terahertz wave sensing with metamaterials," *Opt. Express*, Vol. 19, 21620, 2011.
14. He, X.-J., Y. Wang, J. Wang, T. Gui, and Q. Wu, "Dual-band terahertz metamaterial absorber with polarization insensitivity and wide incident angle," *Progress In Electromagnetics Research*, Vol. 115, 381–397, 2011.
15. Ding, F., J. Dai, Y. Chen, J. Zhu, Y. Jin, and S. I. Bozhevolnyi, "Broadband near-infrared metamaterial absorbers utilizing highly lossy metals," *Scientific Reports*, Vol. 6, Article number: 39445, 2016.
16. Liu, Y., S. Gu, and C. Luo, "Ultra-thin broadband metamaterial absorber," *Appl. Phys. A*, Vol. 108, 19–24, 2012.
17. Tao, H., N. I. Landy, C. M. Bingham, X. Zhang, R. D. Averitt, and W. J. Padilla, "A metamaterial absorber for the terahertz regime: Design, fabrication and characterization," *Opt. Express*, Vol. 16, 7181, 2008.
18. Wen, Q. Y., H. W. Zhang, Y. S. Xie, Q. H. Yang, and Y. L. Liu, "Dual band terahertz metamaterial absorber: Design, fabrication, and characterization," *Appl. Phys. Lett.*, Vol. 95, 241111, 2009.
19. Cheng, Y. H., M. L. Huang, H. R. Chen, Z. Z. Guo, X. S. Mao, and R. Z. Gong, "Ultrathin six-band polarization-insensitive perfect metamaterial absorber based on a cross-cave patch resonator for terahertz waves," *Materials*, Vol. 10, No. 6, 591, 2017.
20. Huang, M., Y. Cheng, Z. Cheng, H. Chen, X. Mao, and R. Gong, "Based on graphene tunable dual-band terahertz metamaterial with wide-angle," *Opt. Commun.*, Vol. 415, 194–201, 2018.
21. Luo, H. and Y. Cheng, "Dual-band terahertz perfect metasurface absorber based on bi-layered all dielectric resonator structure," *Opt. Mater.*, Vol. 96, 109279, 2019.
22. Ju, Z. D., G. Q. Xu, Z. H. Wei, J. Li, Q. Zhao, and J. Huang, "A single-patterned five-band terahertz metamaterial absorber based on multiple resonance mechanisms," *Mod. Phys. Lett. B*, Vol. 32, 1850029, 2018.
23. Wang, B. X., G. Z. Wang, and L. L. Wang, "Design of a novel dual-band terahertz metamaterial absorber," *Plasmonics*, Vol. 11, 523–530, 2016.
24. Yahiaoui, R., S. Tan, L. Cong, R. Singh, F. Yan, and W. Zhang, "Multispectral terahertz sensing with highly flexible ultrathin metamaterial absorber," *J. Appl. Phys.*, Vol. 118, 083103, 2015.
25. Zhu, J., Z. Ma, W. Sun, F. Ding, Q. He, L. Zhou, and Y. Ma, "Ultra-broadband terahertz metamaterial absorber," *Appl. Phys. Lett.*, Vol. 105, 021102, 2014.
26. Wen, Y., W. Ma, J. Bailey, G. Matmon, and X. Yu, "Broadband terahertz metamaterial absorber based on asymmetric resonators with perfect absorption," *IEEE Trans. on Terahertz Science and Technology*, Vol. 5, 406–411, 2015.
27. Wang, G. D., M. H. Liu, X. W. Hu, L. H. Kong, L. L. Cheng, and Z. Q. Chen, "Broadband and ultra-thin terahertz metamaterial absorber based on multi-circular patches," *Eur. Phys. J. B*, Vol. 86, 2013.
28. Ju, Z. D., G. Q. Xu, Z. H. Wei, J. Li, Q. Zhao, and J. Huang, "An ultra-broadband terahertz metamaterial absorber based on split ring array and island-shape structures," *Mod. Phys. Lett. B*, Vol. 32, 1850189, 2018.

29. Cheng, Y., R. Gong, and Z. Cheng, "A photoexcited broadband switchable metamaterial absorber with polarization-insensitive and wide-angle absorption for terahertz waves," *Opt. Commun.*, Vol. 361, 41–46, 2016.
30. Cheng, Y., R. Gong, and J. Zhao, "A photoexcited switchable perfect metamaterial absorber/reflector with polarization-independent and wide-angle for terahertz waves," *Opt. Mater.*, Vol. 62, 28–33, 2016.
31. Huang, M. L., Y. Z. Cheng, Z. Z. Cheng, H. R. Chen, X. S. Mao, and R. Z. Gong, "Design of a broadband tunable terahertz metamaterial absorber based on complementary structural graphene," *Materials*, Vol. 11, No. 4, 540, 2018.
32. Li, D., H. Huang, H. Xia, J. Zeng, H. Li, and D. Xie, "Temperature-dependent tunable terahertz metamaterial absorber for the application of light modulator," *Results Phys.*, Vol. 11, 659–664, 2018.
33. Zhou, S., Z. Shen, R. Kang, S. Ge, and W. Hu, "Liquid crystal tunable dielectric metamaterial absorber in the terahertz range," *Appl. Sci.*, Vol. 8, 2211, 2018.
34. Grant, J., Y. Ma, S. Saha, A. Khalid, and D. R. Cumming, "Polarization insensitive, broadband terahertz metamaterial absorber," *Opt. Lett.*, Vol. 36, 3476, 2011.
35. Hu, F., L. Wang, B. Quan, X. Xu, Z. Li, Z. Wu, and X. Pan, "Design of polarization insensitive multiband terahertz metamaterial absorber," *J. Phys. D: Appl. Phys.*, Vol. 46, 2013.
36. Valagiannopoulos, C. A., A. Tukiainen, T. Aho, T. Niemi, M. Guina, S. A. Tretyakov, and R. Simovski, "Perfect magnetic mirror and simple perfect absorber in the visible spectrum," *Phys. Rev. B*, Vol. 91, 115305, 2015.
37. Papadimopoulos, A. N., N. V. Kantartzis, N. L. Tsitsas, and C. A. Valagiannopoulos, "Wide-angle absorption of visible light from simple bilayers," *Appl. Optics*, Vol. 56, 9779–9786, 2017.
38. Ra'di, Y., V. S. Asadchy, and S. A. Tretyakov, "Total absorption of electromagnetic waves in ultimately thin layers," *IEEE Trans. Antennas Propag.*, Vol. 61, 4606–4614, 2013.
39. Tagay, Z. and C. Valagiannopoulos, "Highly selective transmission and absorption from metasurfaces of periodically corrugated cylindrical particles," *Phys. Rev. B*, Vol. 98, 115306, 2018.
40. Nefedov, I. S., C. A. Valagiannopoulos, and L. A. Melnikov, "Perfect absorption in graphene multilayers," *J. Opt.*, Vol. 15, 114003, 2013.
41. Lei, L., S. Li, H. Huang, K. Tao, and P. Xu, "Ultra-broadband absorber from visible to near-infrared using plasmonic metamaterial," *Opt. Express*, Vol. 26, 5686, 2018.